IPEM Institute of Physics and Engineering in Medicine

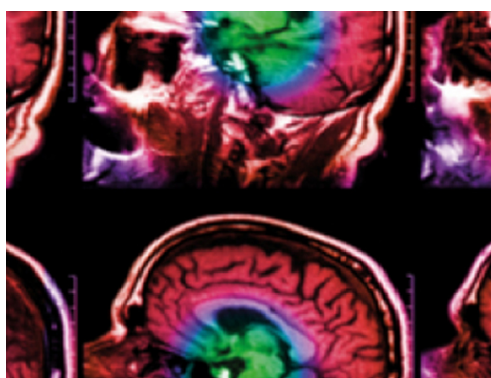**PAPER • OPEN ACCESS**

The role of flow rotation in the adult right atrium: a 4D flow cardiovascular magnetic resonance study

View the article online for updates and enhancements.

Physiological Measurement

IPEM | Institute of Physics and Engineering in Medicine

CrossMark

OPEN ACCESS

PAPER

The role of flow rotation in the adult right atrium: a 4D flow cardiovascular magnetic resonance study

Peter Dewhurst[1], Louise Coats[2,3], Jehill D Parikh[4], Kieren G Hollingsworth[4] and Lian Gan[1] (iD)

1   Department of Engineering, Durham University, Durham, DH1 3LE, United Kingdom of Great Britain and Northern Ireland
2   Institute of Genetic Medicine, Newcastle University, Newcastle upon Tyne, NE1 3BZ, United Kingdom of Great Britain and Northern Ireland
3   Freeman Hospital, Newcastle upon Tyne, NE7 7DN, United Kingdom of Great Britain and Northern Ireland
4   Newcastle Magnetic Resonance Centre, Institute of Cellular Medicine, Newcastle University, Newcastle upon Tyne, NE4 5PL, United Kingdom of Great Britain and Northern Ireland

E-mail: lian.gan@durham.ac.uk

Abstract

Objective: In healthy adults, the right atrium (RA) serves as a reservoir for the systemic flow return from the superior vena cava (SVC) and inferior vena cava (IVC), preparing the two flows to be transferred to the right ventricle (RV) and pulmonary circulation. This study aims to quantify the haemodynamics of the RA and the associated SVC and IVC inflows, which have not been fully understood to date. *Approach*: Eighteen adults with structurally normal hearts underwent 4D flow magnetic resonance imaging. The cardiac cycle was resolved to 20 temporal phases with a spatial resolution of $3 \times 3 \times 3$ mm^3. Analysis included objective visualisation of the flow structures in the RA identified by three different vortex identification criteria, kinetic energy (KE), enstrophy and dissipation. KE and helicity flux were also assessed in both caval veins. *Main results*: Vortex identification methods confirmed that in the majority of participants the blood flow from the caval veins filling the RA during ventricular systole is not chaotic, but rather forms an organised pattern of a single coherent forward turning vortex structure. Thirteen participants displayed a single vortex flow structure, four showed multiple vortices and one had a helical flow pattern without a clear vortex structure. A strong positive correlation exists between the flow KE and enstrophy density. *Significance*: This suggests that flow energy in the RA is mainly rotational, part of which is convected by the highly helical SVC and IVC inflows. Multiple vortices tend to be associated with higher dissipation rates in the central RA region due to turbulence. The rotational nature of the flow in the RA maintains KE better than non-rotational flow. RA flow characteristics are highly related to the helicity content in the caval veins, as well as the KE flux intensity. Lower caval helicity or IVC KE flux dominance tends to favour single vortex formation while the opposite tends to lead to multiple vortices or the rare helical flow patterns. Atria lacking single vortex flow are inclined to have a larger energy input from atrial contraction.

1. Introduction

The right atrium (RA) forms the interface for deoxygenated blood to pass from the superior and inferior vena cava (SVC and IVC) to the right ventricle (RV) for circulation through the pulmonary system. There has been extensive research into the characteristic flows within the left side of the heart (Eriksson *et al* 2011, Töger *et al* 2012, Pedrizzetti and Domenichini 2005, Fluckiger *et al* 2013) and the RV (Carlsson *et al* 2012, Selton-Suty and Juilliére 2009), however flow through the RA is often overlooked despite being of great clinical importance. For example, many heart defects can be detected from abnormalities in RA size and function (Fluckiger *et al* 2013, Sallach *et al* 2009, Meng *et al* 2017, Markl *et al* 2016). In previous studies, evaluation of the fluid dynamics within the RA mainly has been qualitative (Parikh *et al* 2017,

Kilner *et al* 2000, Suwa *et al* 2014). Although this is useful for examining the generic flow regimes within the RA, there is very little as yet which quantitatively characterises flow in the RA. There has been increasing interest in the role of rotational flow within the heart and how it contributes to cardiac function (Martínez-Legazpi *et al* 2014, Watanabe *et al* 2008, Kilner 2010, Watanabe *et al* 2010, Arvidsson *et al* 2013). Kilner *et al* (2000) theorised that the looped shape of the heart aids in the conservation of fluid momentum, improving its efficiency. They found that in the RA incoming flows from the IVC and SVC did not collide with each other, as one might expect, but instead interacted with one another in a circular motion. It was hypothesised that this helps the flow maintain its momentum and redirect itself towards the RV, requiring less external work to be done on the fluid. This investigation used streamlines and flow visualisation to show this phenomenon, however, without quantitative analysis.

Similarly, rotational flow has been linked to healthy heart function (Suwa *et al* 2014). Patients with vortex structures within the left atrium (LA) had fewer organic heart diseases and larger peak flow velocities compared to patients whose incoming blood flows collided rather than rotated. One concern with colliding flows is the possibility of blood stagnation; a prominent feature of a variety of heart conditions and associated with thrombus formation (Markl *et al* 2016, Töger *et al* 2012, Fyrenius *et al* 2001). It might thus be inferred that rotational flow and the interaction of the SVC and IVC in the RA may also contribute. Again, it was suggested that the vortex formed in the LA may be linked to improved efficiency as blood moves from the pulmonary veins to the left ventricle (LV). Suwa *et al* (2014) has little quantitative data and relies on assumptions based on flow visualisation.

Quantitative data to support the hypothesis of rotational flow improving heart efficiency has been explored in other research. Martínez-Legazpi *et al* (2014) quantifies the efficiency benefits of vortex formation on LV filling. It was found that up to 15% of LV volume could be filled with no energetic cost to the heart. Energy of the intracardiac blood flow is provided through two key mechanisms: contraction of the cardiac chambers and the kinetic energy (KE) of the flow itself. The former requires additional energy input to the system, but the latter is a quantity that can be largely conserved by the flow, requiring less work input to maintain and therefore improving the efficiency of the heart. This suggests the importance of rotational flow in the LV. Whilst KE plays a less important role in cardiac function at rest, it has been shown to be of great importance during exercise as heart rate increases (Carlsson *et al* 2012, Kilner *et al* 1997, Prec *et al* 1949). Understanding the KE production and maintenance within the RA is therefore fundamentally helpful in understanding the physiology of RA.

Arvidsson *et al* (2013) examined the KE within the LA and RA. It was found that KE in the LA was appreciably lower than the RA, hence it was proposed that the KE and the momentum of blood flow within the RA has a more important contribution to ventricular filling than the LA which relies more heavily on atrial contraction. They hypothesised a hydraulic flywheel within the RA, conserving KE as it is passed to the RV. The KE, however, is a scalar quantity and takes no account of flow velocity direction or the degree to which the flow within the RA is rotating. That is, a parallel flow stream can have the same KE as a flow undergoing strong rotational motion. Whilst the importance of KE is supported by Eriksson *et al* (2011), it is under debate whether strictly only rotational KE plays a key role in cardiac function (Carlsson *et al* 2012). There is therefore a missing link between these works, namely whether or not the flow rotation is connected to its KE.

Organised vortex structures are known to be adopted to improve the efficiency of fluid mass transport in some biological systems (Dabiri and Gharib 2005). The shape of the heart has evolved to optimise such vortex structure formation, e.g. vortex ring in the LV (Pedrizzetti and Domenichini 2005, Arvidsson *et al* 2016). Vortex structures within the human heart, however, have been found to be far more complex than simple ring shapes. An examination of flow within the LV by Töger *et al* (2012) found additional complexity within the vortex structures produced compared to that in idealised *in vitro* experiments. They also noted that vortex structures appeared not to be present in certain anatomical views, which questions the validity of flow visualisation techniques to define flow regimes. Parikh *et al* (2017), which this paper builds on, identified multiple vortex and helical streamline patterns within the RA, attributing this to positioning of the caval veins. It seems important, therefore, to not only examine how KE relates to the flow within the RA but also to evaluate the helicity (a measure of the helical intensity) and enstrophy (a measure of the rotational energy) to try to establish quantitative relationships within this complex flow regime.

Several methods of examining flow within the human heart have been used previously including echocardiography (Meng *et al* 2017, Hong *et al* 2008, Ruski *et al* 2010), computational modelling of virtual heart chambers (Watanabe *et al* 2008), and Doppler ultrasound methodologies (Kilner *et al* 1997). There also has been an *in vitro* measurement on a right heart phantom model, where laboratory laser based measurement was performed to evaluate vortex structures and wall shear stresses (Gülan *et al* 2017). The present work uses data taken from time-resolved, three-dimensional velocity encoded magnetic resonance imaging (4D flow MR). This technique has been employed in previous studies (Töger *et al* 2012, Fluckiger

et al 2013, Carlsson *et al* 2012, Markl *et al* 2016, Arvidsson *et al* 2013, Markl *et al* 2011) and the findings have been shown to correlate with data acquisition from alternative methods (Markl *et al* 2012). It is considered a suitable *in vivo* technique for measuring volumetric flow velocity data within the cardiac chambers non-invasively, allowing quantification of the predominant flow regimes within an atrium with satisfactory spatial and temporal resolution and accuracy (Fluckiger *et al* 2013).

The aim of this research is to examine the influence of the caval inflow characteristics on the resulting flow structures in the RA.

2. Methods

2.1. Study population
The study population included 18 participants with structurally normal hearts and who were in sinus rhythm (age range 21–50, male: $n = 7$). Nine of them (male: $n = 3$) had cyrptogenic stroke or transient ischaemic attack and patent foramen ovale confirmed by trans-oesophageal echocardiography, which are not believed to have important impact on normal cardiac functions. This study group was prospectively recruited between May 2013 and May 2015. Newcastle and North Tyneside 2 Ethics committee approved the study (12/NE/0140). All participants gave informed written consent.

2.2. Magnetic resonance imaging
MRI was performed at 3.0 Tesla (Achieva, Philips Best, The Netherlands) with a cardiac phased array coil. Multi-slice, multi-phase fast-field echo cine scans in three orthogonal planes were acquired during free breathing for an anatomical overview and to facilitate subsequent planning. The 4DMR was performed using a retrospectively ECG-gated and respiratory gated turbo field echo sequence (TR/TE/flip: 6.3 ms/3.7 ms/8°, VENC: 150 m s^{-1}, FOV: 240 mm (antero-posterior) × 240 mm (inferior-superior) × 142 mm (left-right), spatial resolution: $3 \times 3 \times 3$ mm^3, temporal resolution: 50–55 ms, 20 phases (*Ph*) in a cardiac cycle, SENSE factor 2 and turbo factor 2. A respiratory navigator was employed to reduce motion artefact (navigator efficiency was 60–70%, sequence duration 18.8 ± 3.5 min). Phase errors introduced by eddy currents and Maxwell terms were corrected during the reconstruction process (Carlsson *et al* 2011).
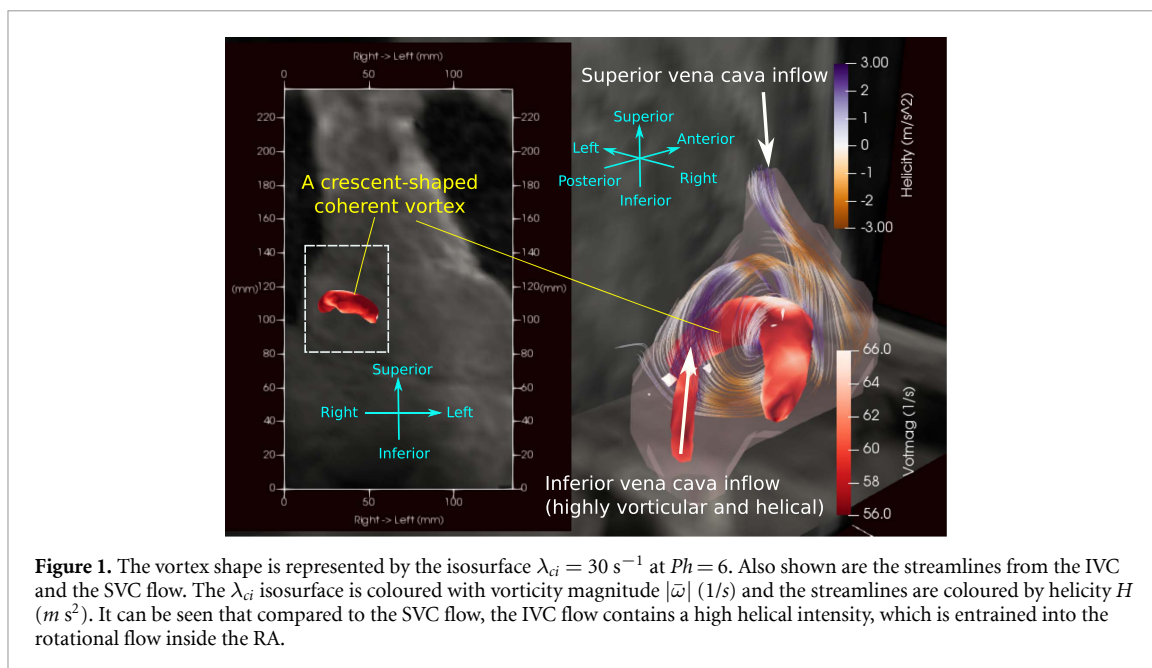
2.3. Data analysis
Three-dimensional segmentation of the RA geometry was performed manually for each of the 20 phases of each participant using GT-Flow v2.2 (Gyrotools) and Matlab (The MathWorks Inc.). This aimed to segment the RA cavity, as well as the IVC and SVC at the caval-RA junction planes for each phase, so that the dependence of their size on the cardiac phase is taken into consideration. The mathematical definitions of the haemodynamic quantities that will be investigated are provided in appendix A.

In addition to the total flow kinetic energy E_k (equation (A1)), which is a quantity usually of interest, the total vorticity energy, namely the enstrophy E_s, is evaluated in the current work. Enstrophy is a measure of the rotational energy which is calculated by equation (A3). Vorticity is the local rotation (spin) rate of a fluid element (equation (A2)). It must be emphasised that the bulk flow could rotate about a centre with zero local vorticity, e.g. a tornado or a flow to a sink. In such flows, which are often called free vortex flow, E_k could be large but E_s is zero except at the centre of rotation. The flow is just swept around rather than (actively) rotating.

Helicity is a measure of how helical a flow is and is calculated by equation (A4). It is an important contribution to the rotational energy in a flow especially for that in a confinement such as in the RA and in the caval veins. A flow element has non-zero helicity if it has non-zero vorticity and at the same time is moving in the direction not entirely perpendicular to the vorticity (rotation) axis. Total helicity content E_h is calculated by equation (A5).

While developing, KE of a flow is continuously dissipated due to the combined effect of blood viscosity and shear (velocity gradient). The rate at which it is dissipated in a flow as a whole is denoted as E_ϵ and can be calculated by equation (A6). It acts as the drain of the flow KE.

It is plausible that E_k, E_s, E_h in the RA originate from SVC and IVC inflow and are all dependent on temporal phase. Since the bulk flow in the two caval veins are almost unidirectional to the RA, the KE flux $\dot{E}$ is used to measure the energy input rate from the caval veins to the RA, and is calculated by equation (A10). Similarly, the vorticity energy that is delivered to the RA is quantified by helicity flux $\dot{H}$; see equation (A11). It is also expected that they are largely proportional to the RA volume, while $\dot{E}$ and $\dot{H}$ are proportional to the vein diameter, which are highly variable among individuals. In this paper, these quantities are normalised by the RA volume and/or the IVC/SVC size. The RA volume was calculated directly from the phase (time) dependent volume, rather than using the maximum volume estimated at ventricular systole

Figure 1. The vortex shape is represented by the isosurface $\lambda_{ci} = 30\ s^{-1}$ at $Ph = 6$. Also shown are the streamlines from the IVC and the SVC flow. The λ_{ci} isosurface is coloured with vorticity magnitude $|\bar{\omega}|$ $(1/s)$ and the streamlines are coloured by helicity H $(m\ s^2)$. It can be seen that compared to the SVC flow, the IVC flow contains a high helical intensity, which is entrained into the rotational flow inside the RA.

(Maceira *et al* 2013). In this way, the normalised quantities remove the size dependence on temporal phase and only reflect the haemodynamic characteristics, and therefore are *densities*.

2.4. Vortex identification

In order to confirm the existence of organised vortex structures in the RA during the cardiac cycle, we carried out a criteria independence check, which is presented in appendix B. It is evident from this that the geometry of the vortex does not depend on the visualisation criteria. The swirling strength (λ_{ci}) criterion is adopted to visualise vortex structures. An example is shown in figure 1. The distribution pattern of the streamlines around the vortex suggests that for this particular case, the vortex is formed by the rolling up of the IVC inflow whilst the SVC inflow seems much weaker and does not have much influence. This is similar to the vortical pattern classified in Parikh *et al* (2017). The RA geometry also has an impact on the vortex shape.

We classified coherent vortex structures found as being one of two distinct types, namely single vortex and multiple vortices. Single vortex flow was defined as a single, centralised vortex originating from IVC flow with SVC flow wrapping around the outside of the vortex structure, typically observable during ventricular systole (atrial filling), similar to that shown in figure 1. A participant was considered as having multiple vortices when at least two vortices of comparable size appear at peak atrial filling (e.g. $Ph = 7$). Cases containing multiple vortices do not display the strong IVC KE flux dominance as observed in single vortex cases.
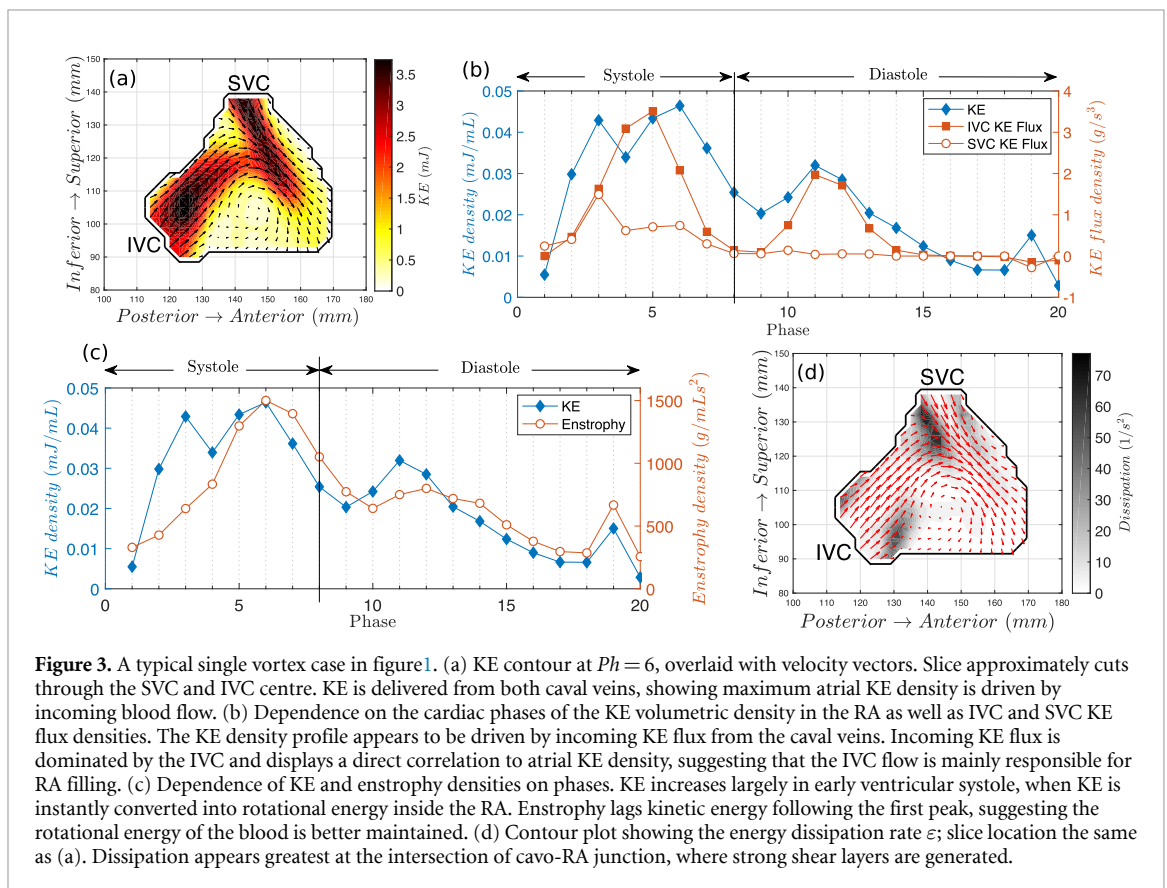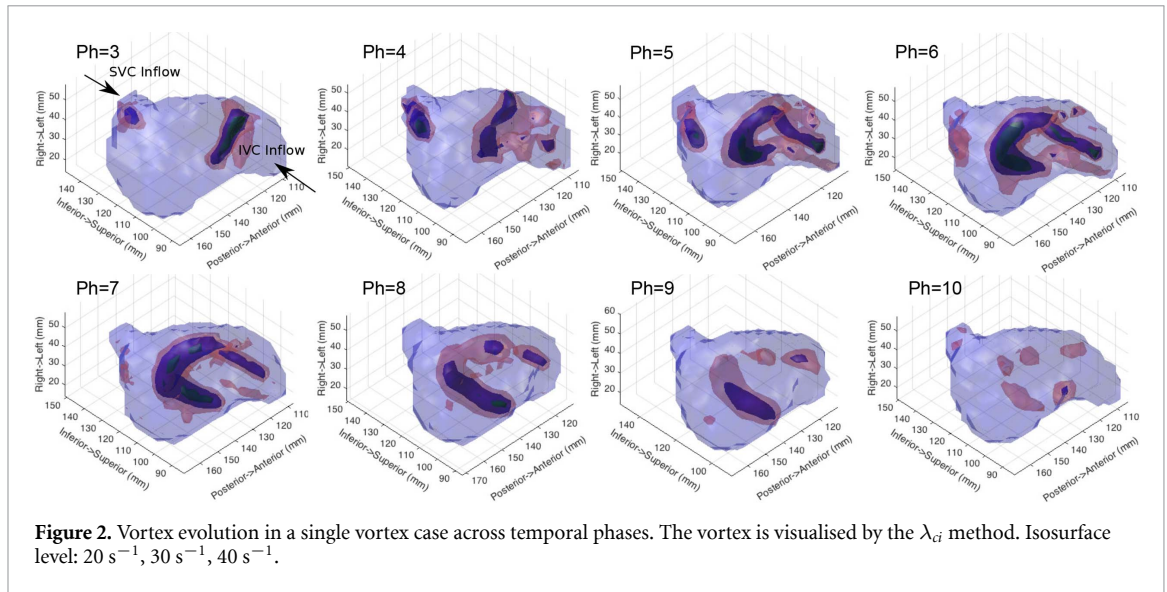
3. Results

Among the 18 participants studied, 13 displayed single vortex flow, four displayed multiple vortices and only one showed a helical flow streamline pattern without an identifiable coherent vortex formed. The four participants with multiple vortices all had patent foramen ovale. Presented below is a typical example of the single vortex pattern, as has been observed previously (Kilner *et al* 2000, Arvidsson *et al* 2013) and three multiple vortices cases of RA flows.

3.1. Single vortex cases

Figure 1 shows the crescent-shaped vortex formed at peak atrial filling for a typical participant having single vortex. The evolution of this vortex is illustrated in figure 2; see also the attached multimedia. This vortex is dissipated after $Ph = 10$, as no coherent vortex of the same strength can be observed after.

SVC blood flow is forced to pass around the vortex to the outside, whereas IVC flow curls in forming the vortex. It appears that the IVC flow dominates the SVC flow and is the main contributor to RA filling. This is confirmed by examining figure 3(b) which shows that the KE volumetric density in the RA is aligned with the IVC flux, while the SVC flux is at appreciably lower intensity. It is expected given the IVC is responsible for transport of a much larger volume of blood than the SVC. Atrial KE displays three distinct local peaks, the highest peak occurs during ventricular systole ($Ph = 3 \sim 6$, denoted as systolic peak) and two smaller

Figure 2. Vortex evolution in a single vortex case across temporal phases. The vortex is visualised by the λ_{ci} method. Isosurface level: $20\,\mathrm{s}^{-1}$, $30\,\mathrm{s}^{-1}$, $40\,\mathrm{s}^{-1}$.

Figure 3. A typical single vortex case in figure 1. (a) KE contour at $Ph = 6$, overlaid with velocity vectors. Slice approximately cuts through the SVC and IVC centre. KE is delivered from both caval veins, showing maximum atrial KE density is driven by incoming blood flow. (b) Dependence on the cardiac phases of the KE volumetric density in the RA as well as IVC and SVC KE flux densities. The KE density profile appears to be driven by incoming KE flux from the caval veins. Incoming KE flux is dominated by the IVC and displays a direct correlation to atrial KE density, suggesting that the IVC flow is mainly responsible for RA filling. (c) Dependence of KE and enstrophy densities on phases. KE increases largely in early ventricular systole, when KE is instantly converted into rotational energy inside the RA. Enstrophy lags kinetic energy following the first peak, suggesting the rotational energy of the blood is better maintained. (d) Contour plot showing the energy dissipation rate ε; slice location the same as (a). Dissipation appears greatest at the intersection of cavo-RA junction, where strong shear layers are generated.

peaks at $Ph = 11$ (early diastolic peak), 19 (late diastolic peak), which are atrial contraction. It is worth mentioning that for this particular participant and a few others (e.g. the one in section 3.3, multiple vortices case 2), it shows an additional early systolic peak at $Ph = 3$. No abrupt change of atrial volume or velocity magnitude was observed at $Ph = 3 \sim 5$, nor is it a consistent behaviour observed in other single vortex cases. The aligned systolic peak and early diastolic peak indicate two surges in RA filling, compared to the SVC which displays a much smaller peak at systole. The alignment of these peaks suggests that the KE in the RA is driven by the caval vein inflow, rather than the contraction/relaxation of the muscular walls.

The smaller late diastolic KE peak at $Ph = 19$ relates to atrial contraction leading to reduced RA volume as KE flux from the caval veins are low. This is consistent in all the participants. The larger IVC KE flux over the cardiac cycle demonstrates that in the typical RA, blood intake from the IVC dominates RA filling and SVC flow plays a minor role in comparison.
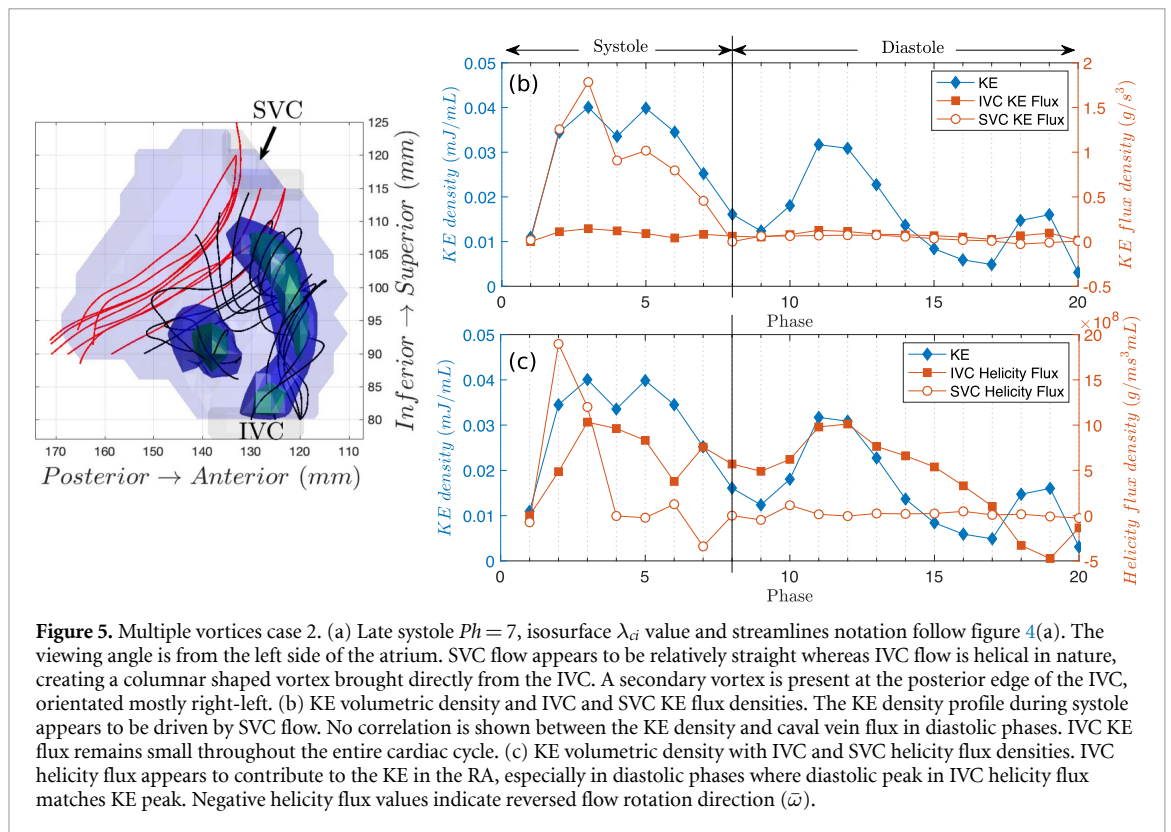
Figure 4. Multiple vortices case 1. (a) $Ph = 7$, isosurface of λ_{ci} values (blue: $\lambda_{ci} = 30 \text{ s}^{-1}$, green: $\lambda_{ci} = 40 \text{ s}^{-1}$) and 90th percentile KE values (red). Black streamlines show the direction of flow from the IVC, red streamlines show the direction of flow from the SVC. Maximum KE values appear to come straight from the SVC creating two vortices, one strong SVC vortex and one smaller IVC vortex. (b) $Ph = 14$, colour codes for isosurfaces and streamlines follow (a). The stronger IVC KE flux creates a small vortex at the anterior edge of the IVC opening. The evolution of the vortices can be found in the attached multimedia. (c) KE volumetric density with IVC and SVC KE flux densities. The KE density profile appears to be dominated by SVC flow during systolic peak at $Ph = 8$. IVC flow grows in strength during the diastolic phases, returning the flow structure to a weak single vortex.

Examination of the KE intensity distribution within the RA (figure 3(a)) provides further support that RA KE is from the caval intakes. At this particular phase, KE is shown to come from both caval veins but no substantial atrial volumetric change was observed. The in-plane velocity vector pattern casts more light on the stream pattern shown in figure 1. The vortex rolls up beneath the IVC stream as it encounters the barrier created by the energetic SVC stream and only a small portion of the SVC flow is entrained into the vortex core.

The behaviour of the enstrophy density in figure 3(c) shows that the systolic KE peak is approximately synchronised with the high rotational energy of the flow. Figure 3(d) shows that the strongest dissipation intensity occurs where the IVC current meets the SVC current at the posterior of the SVC intake. Whilst the SVC flow remains largely straight, this flow pattern creates a sharp velocity gradient and thus an intense shear layer. Rather weak dissipation is seen within and around the central rotating vortex, which infers the role of rotational flow in maintaining the energy of the blood flow in such a flow configuration. Some strong dissipation was also observed at the posterior edge of the vortex where the bulk rotating flow encounters the incoming IVC blood flow, also creating a strong shear locally. It is plausible that this allows the incoming IVC blood to accelerate stagnant blood and reintroduce it into the vortex.

While the vortex pattern and KE enstrophy behaviours are consistent in all 13 participants with single vortex in the RA, the multiple vortices cases are found to be heterogeneous in the vortex structures and the associated haemodynamic quantities. Discussed next are three of the four cases where multiple vortices are formed by different mechanisms. We also observed one case where the incoming blood flow from the caval veins fails to form any coherent vortex but instead winds round one another in a helical manner. This helical flow case will not be discussed in detail here.

3.2. Multiple vortices: case 1

Figure 4(c) shows the atrial KE density and KE flux intensity from both caval veins for a participant having multiple vortices. During atrial filling, the SVC blood flow appears to be the main contributor to the atrial KE, which maximises at late systole ($Ph = 8$). IVC KE flux slowly increases without displaying any identifiable peak throughout the cardiac cycle and eventually overtakes the SVC KE flux during diastolic filling. Peak values of the SVC KE flux are comparable to that in the single vortex case (note different axis range), both being around 1 g s^{-3} and only IVC flow is restricted, which stays at a low magnitude for the entire cardiac

Figure 5. Multiple vortices case 2. (a) Late systole $Ph = 7$, isosurface λ_{ci} value and streamlines notation follow figure 4(a). The viewing angle is from the left side of the atrium. SVC flow appears to be relatively straight whereas IVC flow is helical in nature, creating a columnar shaped vortex brought directly from the IVC. A secondary vortex is present at the posterior edge of the IVC, orientated mostly right-left. (b) KE volumetric density and IVC and SVC KE flux densities. The KE density profile during systole appears to be driven by SVC flow. No correlation is shown between the KE density and caval vein flux in diastolic phases. IVC KE flux remains small throughout the entire cardiac cycle. (c) KE volumetric density with IVC and SVC helicity flux densities. IVC helicity flux appears to contribute to the KE in the RA, especially in diastolic phases where diastolic peak in IVC helicity flux matches KE peak. Negative helicity flux values indicate reversed flow rotation direction ($\bar{\omega}$).

cycle. Nevertheless, the KE density in the RA shows an appreciably higher peak compared to the single vortex case at late systole. This is because of a smaller RA volume for this particular case.
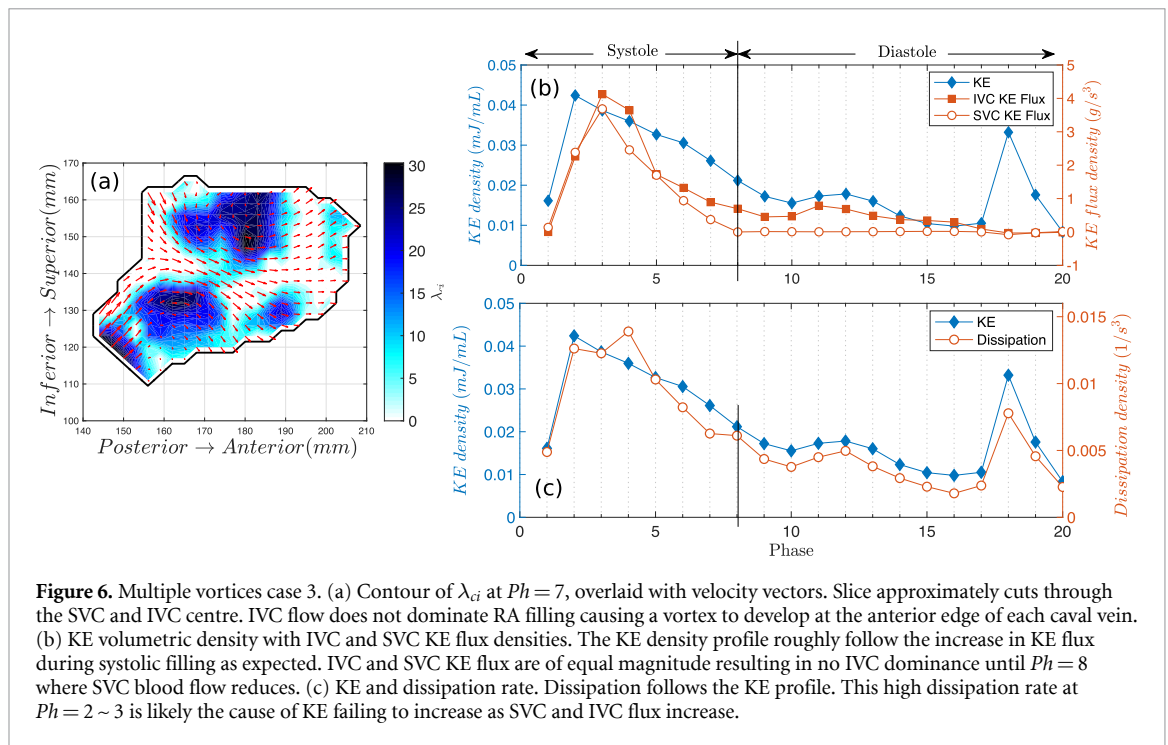
Given that the overall KE flux dominance swaps between SVC and IVC, different flow patterns are expected in systolic and diastolic atrial filling. At $Ph = 7$, where SVC KE flux dominates, two strong and separate vortices are observed; see figure 4(a). The vortices are created at the anterior edge of each caval vein opening and have similar intensity as that in figure 1. The SVC vortex appears much stronger in the vortex core with much higher λ_{ci} values than the IVC vortex. The red isosurface shows the 90th percentile of KE values within the RA at this phase. The KE comes straight from the SVC, driving the flow to rotate. Physical space is limited where the vortex is generated, however, and it may restrict development and easily disrupt the vortex as it interacts with the incoming SVC flow.

The IVC flux overtakes the SVC flux at mid diastole ($Ph \approx 10$) and the vortex associated with the SVC flow vanishes, leaving only a small IVC vortex; see figure 4(b). The 90th percentile of KE values, shown by the red isosurface, indicates that most of KE originating from the SVC flow is maintained at this phase.

3.3. Multiple vortices: case 2

This participant presents formation of multiple vortices due to the blood flow within the IVC being highly helical. Figure 5(b) shows that there appears to be a very strong KE flux from SVC during systole and IVC KE flux remains small throughout. The systolic peak, therefore, should be a result of the strong SVC input. However, it suggests that the diastolic peak is not directly associated with KE flux from either SVC or IVC. According to equation (A10), KE flux mainly takes into account the energy carried by parallel streams, but not the rotation of the flow entering the RA. Indeed, the helicity flux profile in figure 5(c) implies that the early diastole KE peak ($Ph \approx 11$) is supplied from the IVC helicity flux instead of KE flux. That is, the IVC flow entering the RA is highly rotational without a strong forward motion. Apparently, this rotation is developed upstream in the IVC. Furthermore, the weak KE peak at late diastole ($Ph \approx 19$) also coincides with an IVC helicity flux peak (negative), although the rotation of the IVC flow is reversed in direction.

Visualisation of the vortices present in figure 5(a) confirms that the bulk rotation is developed within the IVC. The anterior vortex, orientated in the inferior-superior direction, was observed to come directly from the IVC and was not created within the RA. This is fundamentally different to the formation of the single vortex in figures 1 and 3. The highly helical nature of the IVC flow is clearly seen by the streamlines, albeit a very low KE flux at this phase; see (b). Interestingly, at this phase ($Ph = 7$), SVC KE flux is stronger, but no vortex associated with it having similar strength as the IVC one is observed. As the vortex interacts with the relatively straight SVC flow, the vortex collapses and blood follows the SVC blood stream. A secondary vortex

Figure 6. Multiple vortices case 3. (a) Contour of λ_{ci} at $Ph = 7$, overlaid with velocity vectors. Slice approximately cuts through the SVC and IVC centre. IVC flow does not dominate RA filling causing a vortex to develop at the anterior edge of each caval vein. (b) KE volumetric density with IVC and SVC KE flux densities. The KE density profile roughly follow the increase in KE flux during systolic filling as expected. IVC and SVC KE flux are of equal magnitude resulting in no IVC dominance until $Ph = 8$ where SVC blood flow reduces. (c) KE and dissipation rate. Dissipation follows the KE profile. This high dissipation rate at $Ph = 2 \sim 3$ is likely the cause of KE failing to increase as SVC and IVC flux increase.

is then created from the broken IVC flow. This secondary vortex appears to be formed due to recirculating flow interacting with the incoming IVC flow, hence oriented right-left. High intensity dissipation was observed in the space between these two vortices (figure not shown), indicating a sink of energy when multiple vortices mutually interact.

3.4. Multiple vortices: case 3

This participant displays multiple vortices due to equally strong IVC and SVC KE flux. Figure 6(a) shows that two vortices are created at the anterior side of both caval veins and develop independently. Both vortices are of similar size and strength. As shown in figure 6(b), the KE profile shows a strong systolic peak, a weak early diastolic peak ($Ph \approx 12$) followed by a very strong late diastolic peak. The systolic peak occurs at $Ph = 2$, about 50 ms (one phase) before the KE flux peaks. This is due to the combined effects of a weak atrial diastole from $Ph = 2$ to 3 and high dissipation rate, shown in (c). Both SVC and IVC KE flux appear similar in magnitude and in phase during systole. The strong shear layer between the two vortices induces intensive local dissipation rate. This leads to a poor KE conservation and quick decay with much a weaker early diastolic peak, compare to the single vortex case in figure 3. The profile of dissipation is found to be in phase with the KE profile, as shown in figure 6(c).

3.5. Rotational energy and dissipation

Figure 7(a) shows an approximate linear correlation between the KE and the enstrophy content in the RA flow for all the cases studied regardless of the different flow patterns presented above. The helical flow case is also included. Here $\langle E_k \rangle$ and $\langle E_s \rangle$ denote the total KE and enstrophy density throughout a cardiac cycle and are calculated using equation (A13). Figure 7(b) presents the helicity content in the IVC and SVC flows, where $\langle |H| \rangle$ denotes the cycle-averaged helicity density magnitude (not flux) calculated by equation (A15). The use of magnitude density removes the flow rotation direction difference and the vein size variation. It is evident that the blood flow is more helical in the IVC than in the SVC, perhaps because of blood stream merging from different directions from the hepatic veins upstream. To find out the exact reason for the helicity is beyond the scope of the current study. A weak correlation between the helicity magnitude in SVC and that in IVC seems to exist.

Dissipation in the single vortex and the multiple vortices cases are given in figure 8(a). The multiple vortex cases show much larger peak dissipation than the single vortex case. A strong correlation exist between the cycle dissipation $\langle \epsilon \rangle$ (equation (A14)) and the enstrophy $\langle E_s \rangle$ (equation (A13)); see figure 8(b). It means that the magnitude of $\langle \epsilon \rangle$ is largely proportional to $\langle E_s \rangle$ in most of the participants, with two multiple vortices cases deviated stronger away from the linear correlation.
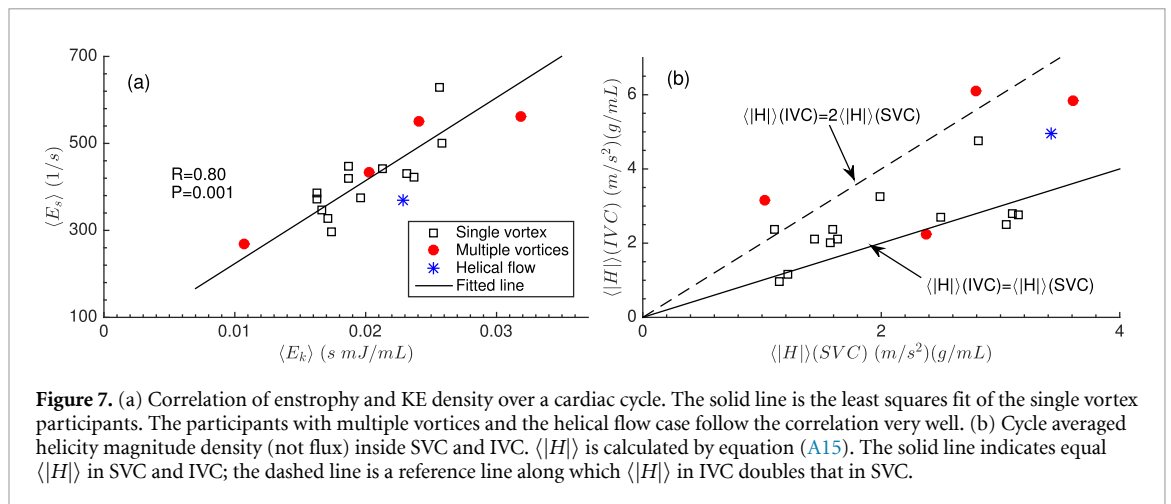
Figure 7. (a) Correlation of enstrophy and KE density over a cardiac cycle. The solid line is the least squares fit of the single vortex participants. The participants with multiple vortices and the helical flow case follow the correlation very well. (b) Cycle averaged helicity magnitude density (not flux) inside SVC and IVC. $\langle |H| \rangle$ is calculated by equation (A15). The solid line indicates equal $\langle |H| \rangle$ in SVC and IVC; the dashed line is a reference line along which $\langle |H| \rangle$ in IVC doubles that in SVC.
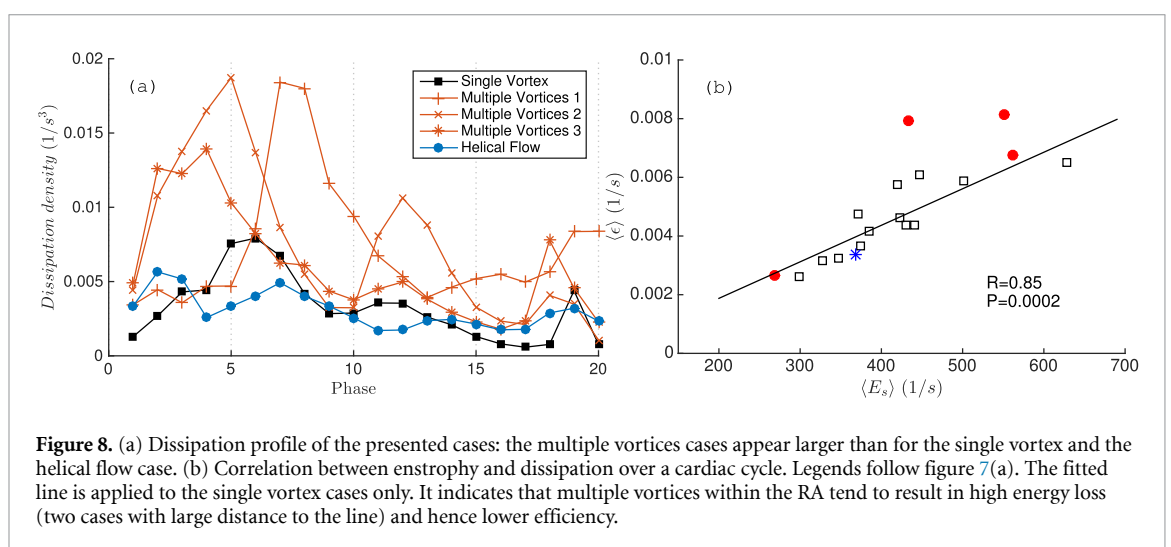
Figure 8. (a) Dissipation profile of the presented cases: the multiple vortices cases appear larger than for the single vortex and the helical flow case. (b) Correlation between enstrophy and dissipation over a cardiac cycle. Legends follow figure 7(a). The fitted line is applied to the single vortex cases only. It indicates that multiple vortices within the RA tend to result in high energy loss (two cases with large distance to the line) and hence lower efficiency.

4. Discussion

In providing a conduit between the caval veins and the RV, the RA, amongst its other functions, preserves the KE whilst redirecting the caval blood flow. Using objective vortex identification methods, two distinctive vortex patterns are identified in the RA, with an additional helical flow pattern where no coherent vortex is observed throughout a cardiac cycle. Different flow patterns primarily depend on the inflow characteristics from the caval veins. IVC dominant KE flux tends to result in a single organised forward rotating vortex commonly observed in the RA during ventricular systole (Kilner *et al* 2000), while the lack of IVC flux dominance tends to lead to the heterogeneous multiple vortices or the rarer helical flow pattern. In addition to the caval veins, the coronary sinus, which drains deoxygenated blood from the cardiac muscle into the RA, also contributes to the RA input. As the flow rate from the coronary sinus is very small (1.5 ± 0.6 ml s^{-1}) (Bloch *et al* 2009) compared to the caval veins (40.3 ± 14.1 and 62.5 ± 17.3 ml s^{-1} for the SVC and IVC respectively) (Parikh *et al* 2017), we believe the coronary sinus does not have much impact on the RA flow structure, and hence have not investigated it here. The coronary sinus opening is located immediately adjacent to the IVC opening and so incoming coronary sinus blood is likely 'swept up' in the much stronger IVC flow.

The presence of a rotating, forward turning vortex in the RA has been well documented in Carlsson *et al* (2012). It is hypothesised that the structural arrangement of the caval veins contributes to the flow pattern (Parikh *et al* 2017). It is apparent, however, that the strength of the incoming flows also appears to contribute. In the majority of participants (72%), the strong IVC KE flux shown in figure 3(b) dominates RA filling, creating the single vortex and expelling SVC blood towards atrium anterior wall. This vortex allows KE to be maintained in rotational motion, redirecting flow from the caval veins towards the tricuspid valve. This permits efficiency of the cardiac output with a large blood through-put capacity and conservation of KE, meaning little energy input is required from the atrium contraction.

This is evidenced by the strong association of the RA KE with the IVC KE intake in the single vortex case (figures 3(a) and (b)). The peak of the IVC flux spans wider systolic phases than the former, which also extends to diastolic phases i.e. atrial KE does not decrease and arise as sharply as IVC KE flux. This indicates that the highly energetic flow in the RA is able to maintain its energy level without input from the caval veins from late systole to early diastole ($Ph = 6 \sim 11$). In addition, the synchronisation of the systolic KE peak and the high rotational energy in figure 3(c) implies that the inflow streaming from the caval veins drives the blood flow in the RA chamber to rotate. That is, KE flux is instantly converted to rotational energy. A small phase lag can be observed between the KE and the enstrophy behaviours, as previously observed (Arvidsson *et al* 2013). This lends support that the vortex seems to be more capable of maintaining energy in a rotating flow.

An important factor of single vortex structures is the influence it has on the SVC flow. Fyrenius *et al* (2001) suggested that a single vortex accelerates the SVC flow moving towards the atrium wall, creating a 'washing' effect and reducing the stasis of atrial blood. If the washing effect supplied by the incoming fresh blood flow is not sufficient, it could facilitate blood stagnation against the atrium walls, which may be hypothesised to contribute to thrombus formation (Markl *et al* 2016, Gülan *et al* 2017). This is more likely to occur in the multiple vortices flow patterns as shown in figures 4, 5 and 6, as well as the helical flow case where no coherent vortex is found. In these cases, SVC flow is also not influenced by the IVC flow to the same extent as in the single vortex participants.

Indeed, the formation mechanism of multiple vortices and helical flows is largely determined by the lost of the IVC flow dominance over the SVC flow. Comparing figures 4(c) and 3(c) shows that even though the peak values of the SVC KE flux in multiple vortices case 1 are comparable to that in the single vortex case, the IVC flow remains at a low magnitude without clear phase dependence. For multiple vortices case 2, figure 5(b) shows that the KE density profile is very similar to the single vortex case (figure 3(b)), but the KE flux profiles from the two caval veins differ greatly with a clear SVC dominance. For multiple vortices case 3, unlike the single vortex case (figure 3(a)) in which the SVC blood was channelled to the outside of a single vortex, assisting its rotation, in this case both flows have similar strength and move away from each other, creating two separate counter rotating vortices and a strong shear layer (velocity gradient) in between.

All four participants displaying multiple vortices are with cryptogenic stroke or transient ischaemic attack and patent foramen ovale confirmed on trans-oesophageal echocardiography. Whether it is merely a coincidence requires a larger sample size to confirm in the future. However, it suggests that the observer independent flow dynamics analysis presented in this work could potentially provide an alternative early diagnosis.

A further role of the looped heart is to redirect blood flow towards the next cardiac chamber. The forward turning vortex in the single vortex cases encourages the redirection of blood from the caval veins towards the tricuspid valve. The counter-rotating SVC vortex observed in figure 4(a) appears to achieve the opposite effect. Red streamlines show the direction of blood from the SVC is drawn away from the tricuspid valve. This is also seen in figure 6(a), where the red arrows from the SVC curl away from the tricuspid valve. Multiple vortices case 2 shows that the main vortex is brought directly from the IVC. This constrains flow towards the posterior side of the RA, again away from the tricuspid valve. If blood is not directed towards the RV, it will likely affect the efficiency of the heart, especially at peak exercise. As the heart rate increases with exercise, the efficient passage of blood becomes increasingly important (Kilner 2010, Kilner *et al* 1997). If flow turns away from the tricuspid valve, this may limit the volume of blood passed to the RV and result in a sub-optimal cardiac output.

In this study, the magnitude of the rotational energy is quantified by enstrophy. It is fundamentally important to differentiate rotational and simple convective flows, which could contain the same amount of KE. The positive correlation between the KE and the enstrophy reflected in figure 7(a) indicates that the flow energy in the RA is maintained in a highly rotational motion both locally and globally, regardless of the flow patterns. The enstrophy in the RA is likely generated in two ways: converted from the existing KE or carried in by the SVC and IVC flow which are highly rotational. Figure 7(b) reveals that flows in the SVC and IVC are not simple pipe flow analogues where streamlines are straight and parallel; rather they are highly helical, which directly contribute to the enstrophy content in the RA. Relatively low helicity in the caval flow, especially in the IVC, tends to result in a single vortex, whilst strong helicity content tends to lead to multiple vortices or helical flow pattern. Nevertheless figure 7(a) suggests that neither $\langle E_k \rangle$ or $\langle E_s \rangle$ alone could convincingly differentiate the three flow patterns observed in the RA.

The decay of KE and enstrophy in the RA is related to dissipation rate or flow to the RV through the tricuspid valve. The latter, associated with the RV and tricuspid valve functions, are not the focus of the current study. Dissipation rate, however, is only related to the haemodynamics in the RA itself. It therefore can be a measure of the output efficiency. Our result found a correlation between the cycle dissipation rate and the enstrophy content in figure 8(b). This is expected since high dissipation intensity usually occurs near

the caval-RA junctions and around the RA wall due to stronger velocity gradient associated with higher rotational strength. It is relatively weak in the central vortex region, meaning that energy is well maintained there; see figure 3(d). However, multiple vortices are associated with a flow pattern which tend to have higher dissipation rate in the central area and a disproportionally higher overall dissipation. The only multiple vortices case with a very low dissipation also has very low overall energy level; see figure 7(a). This implies the morphology of the RA is not optimised for multiple vortices flow to occur. It has been previously suggested that the KE maintained in the RA is directly transferred to the RV with little acceleration of the blood (Arvidsson *et al* 2013, Carlsson *et al* 2012). It therefore is hypothesised that the opening of the tricuspid valve may be sufficient for RV filling due to the rotational energy in the RA, with little RV suction. If this is the case, then the excess dissipation observed in the multiple vortex cases may play an important role in inhibiting RV filling. High dissipation rate in the central area, together with the multiple vortices patterns, also suggests highly chaotic turbulent flows, albeit heterogeneous. This has been shown to (weakly) relate to the elevated pulmonary artery pressure (Wehrum *et al* 2018).

High dissipation was also found to be linked to strong shear originating from vortex interaction, flow-wall interaction as well as vortices obstructing (rather than assisting) incoming flow. If KE is not maintained and delivered efficiently from the caval veins, a greater work input from the atrium wall may be required to assist RV filling. The percentage of peak atrial KE density during atrial contraction (the late diastolic peak) was calculated for all cases. The single vortex case produced an atrial contraction KE of 32% of the systole KE peak, while that for multiple vortices cases 1, 2 and 3 were 67%, 40% and 78%, respectively. This shows a non-trivial increase in RA contraction, especially in cases with competing IVC and SVC KE flux. The helical flow case displayed an atrial contraction KE of 46.53%, 14.14% higher than the single vortex case. All single vortex participants except two (15% of population) have a KE ratio $\lesssim 45\%$ in comparison (mean value: 38%, standard deviation: 22%, with 11 participants having KE ratio of $30\% \pm 5\%$). Whilst this does not appear to be a large increase, examination of the phase dependence of the KE of the RA in the helical flow case (figure not shown) reveals that the maximum KE is formed during early ventricular systole when the tricuspid valve is still closed, but is not well maintained and dropped quickly. Atrial contraction at late diastole ($Ph\approx19$) makes up a larger percentage taken forward into the RV. This implies the heart is having to work harder to move blood from RA to RV. Whilst adaptations due to muscle loading can be desirable in the left side of the heart in terms of improving cardiac output and reducing resting heart rate, over adaptation of the right side of the heart could contribute to cardiac diseases. An increased work rate places unnecessary strain on the heart. Whilst potentially less important at rest, this could increase during exercise and limit cardiac output.

Wehrum *et al* (2018) demonstrated the effect of age on atrial flow patterns. It was found that elderly individuals (60–80 years old) displayed atria with high levels of turbulence without a single clock-wise vortex to form, in contrast to young participants (20–39 years old) who had a clear, single vortex. The cases of multiple vortices presently displayed, however, were all found in patients ranging between 21 and 50 years of age. As the heart ages, cardiac output diminishes and the likelihood of heart diseases is increased. The finding of turbulent flow patterns in younger patients raises the possibility that the presence of multiple vortices could be an early indicator of organic heart diseases.

Parikh *et al* (2017) also suggested that the offset distance between the SVC and IVC, hence the relative the jet angle, is correlated with the qualitative flow patterns in the RA and the group of participants with patent foramen ovale. In the current study we focused our study on the haemodynamic factor rather than the morphological factor, and therefore geometrical variation is not considered.

Future work will be focused on the coupling of the RA flow dynamics with the RV suction work, aiming to provide a more direct evaluation of the impact of the RA flow on the RV output and hence the pulmonary artery pressure and flow efficiency.

5. Limitations

As with most 4D flow MR studies, this work is limited by a lack of population data. Whilst single vortex flow structures appear in 13 of the 18 participants studied, participants with different flow structures are heterogeneous and limited conclusions can be drawn about the mechanisms behind these flow patterns. Current measurement technique also limits the accurate calculation of energy dissipation. Although the large eddy model is a good approximation, this is still constrained by spatial resolution.

Whilst it seems that the RA morphology is apt to the formation of a single coherent vortex during atrial filling, its implications for the cardiac function deserves further study together with other indicative quantities. It has been shown that the maintenance of KE within the heart becomes increasingly important during exercise (Carlsson *et al* 2012, Kilner *et al* 1997, Prec *et al* 1949). Further investigation into flow

structures within the heart during exercise as well as maximum cardiac output are thus needed in order to quantify the positive (or not) effect of single vortex flow in the RA.

6. Conclusions

Blood flow in the RA is highly rotational and it is a universal feature among the 18 participants investigated. Almost all of the KE in the blood flow originating from the two caval veins is in the form of rotational energy which is quantified by enstrophy and is reflected by the correlation of the KE and the enstrophy (figure 7(a)). The rotational energy is largely maintained in the RA regardless of the flow pattern appearance. The blood flow within the two caval veins contains substantial helicity, which directly contributes to the enstrophy and influences the flow patterns within the RA. The IVC flow is in general more helical than the SVC flow. These are confirmed by the helicity flux to the RV from the two caval veins (figure 7(b)). The helicity flux also reveals that if the helicity in the caval veins are of low intensity, the flow pattern in the RA tends to be single vortex type, while high-intensity IVC/SVC helicity or lack of IVC flux dominance (over the SVC flux) tends to result in multiple vortices or helical flow patterns.

It was found that the majority of participants (13) display a distinguishable single vortex structure at ventricular systole. Flow visualisation with streamlines (figure 1) and velocity vectors (figure 3(a)) reveals that typical RA filling is driven by a strong IVC blood intake, which interacts with a weaker SVC intake and create a single centralised vortex containing mainly IVC blood with SVC blood expelled around the outside of the vortex structure. This allows incoming flow from both caval veins to contribute to the same vortex. Atrial contraction appears not to influence the KE content to any great extent. This is indicative of the RA providing an efficient link between the caval veins and the RV.

In the four multiple (two) vortices participants, one vortex is associated with each caval vein intake; see figures 4 to 6. No multiple vortices cases show a dominant IVC KE flux and all cases (except 1) displayed relatively high value of dissipation (figure 8(b)). This suggests the RA is not evolved to optimise blood flows to form multiple vortices, as the two flows are against each other, create a highly turbulent region in the central area and do not maintain the incoming flow energy as well as the single vortex cases, reflected by higher dissipation rate. Among the 18 participants, one was found having no coherent vortex present in the RA throughout the entire cardiac cycle. Blood flow from the two caval veins winds round one another in a helical manner instead (figure not shown). Multiple vortices and helical flow cases tend to have relatively stronger atrial contraction, demonstrated by a higher diastolic KE peak, suggesting inefficiency in flow structures to transfer KE. Such flow patterns therefore could potentially indicate inefficient cardiac output especially during exercise, or be an early disease marker.

Acknowledgment

Appendix A. Haemodynamic quantity calculation

The total KE content within the RA volume is calculated as

$$E_k = \frac{1}{2}\rho \int_{RA} |\bar{u}|^2 \, \mathrm{d}v = \frac{1}{2}\rho \int_{RA} \left(u_1^2 + u_2^2 + u_3^2\right) \, \mathrm{d}v, \tag{A1}$$

where E_k stands for kinetic energy, ρ is the density of blood assumed to be 1.05 g ml^{-1}, v is the RA volume element and (u_1, u_2, u_3) are the velocity component along the three mutually perpendicular principal axes (x_1, x_2, x_3), respectively, which are directly obtained from 4DMR on each voxel.

Vorticity ($\bar{\omega}$) is an important vector quantity to measure the magnitude and the axial direction of spinning of fluid particles in a flow. Similar to velocity, $\bar{\omega}$ has principal components $(\omega_1, \omega_2, \omega_3)$, along (x_1, x_2, x_3), calculated by

$$\bar{\omega} = \left(\frac{\partial}{\partial x_1}, \frac{\partial}{\partial x_2}, \frac{\partial}{\partial x_3} \right) \times (u_1, u_2, u_3)$$
$$= (\omega_1, \omega_2, \omega_3), \tag{A2}$$

where $\times$ is the cross-product of two vector quantities. Whilst KE directly relates to the magnitude of the flow velocity, it does not indicate the rotational strength of a flow. The rotational energy is quantified by enstrophy, calculated as

$$E_s = \frac{1}{2}\rho \int_{RA} |\bar{\omega}|^2 \, \mathrm{d}v = \frac{1}{2}\rho \int_{RA} \left(\omega_1^2 + \omega_2^2 + \omega_3^2 \right) \, \mathrm{d}v. \tag{A3}$$

Helicity (H) is measures how helical a flow is. Helicity is non-zero when the fluid particle is spinning and also moving as a whole at the same time not entirely perpendicular to the spin axis. It is defined as

$$H = \bar{\omega} \cdot \bar{u}, \tag{A4}$$

where $\cdot$ denotes the dot-product of two vectors. Similarly, the total helicity content in the RA is calculated as

$$E_h = \rho \int_{RA} H \, \mathrm{d}v. \tag{A5}$$

In a similar way, energy dissipation is calculated as the volume integral of the local dissipation rate ε,

$$E_\epsilon = \int_{RA} \epsilon \, \mathrm{d}v. \tag{A6}$$

Dissipation occurs at a very small length scale in the flow, typically < 0.1 mm in the RA flow. This is not resolved by the current 4DMR technique. Therefore, we estimate the energy dissipation rate ε using the large eddy model (Smagorinsky J 1963, Sheng *et al* 2000), which is suitable for the present spatial resolution (3 mm). This allows the stress tensor (τ_{ij}) to be modelled as

$$\tau_{ij} = -(C_s \Delta)^2 |\bar{S}| \bar{S}_{ij}, \tag{A7}$$

where Cs is an empirical constant taken to be 0.17, Δ is to model the unresolved small length scales, which takes the value of 3 mm. S_{ij} is the strain rate tensor given by

$$\bar{S}_{ij} = \frac{1}{2} \left(\frac{\partial \bar{u}_i}{\partial x_j} + \frac{\partial \bar{u}_j}{\partial x_i} \right), \tag{A8}$$

where $\partial \bar{u}_i / \partial x_j$ is the velocity gradient at resolved length scales. The subscripts follow the Einstein notation. The energy dissipation rate ε, being the sink of KE, is then calculated as

$$\epsilon_{ij} = -2 \left(\tau_{ij} \bar{S}_{ij} \right). \tag{A9}$$

Here we neglect the blood dynamic viscosity μ, which is a constant $\approx 3 \times 10^{-3}$ sPa.

The rate at which KE is delivered from the caval veins to the RA can be quantified by the KE flux. For instance, the IVC KE flux is calculated as

$$\dot{E}_{IVC} = \rho \int_{IVCS} \bar{u}^2 \left(\bar{u} \cdot \bar{n} \right) \, \mathrm{d}s, \tag{A10}$$

where $\bar{n}$ is the unit vector pointing normally to the RA at the IVC-RA junction plane and s is the plane surface element. Similarly, helicity flux can be calculated as

$$\dot{H}_{IVC} = \rho \int_{IVCS} H (\bar{u} \cdot \bar{n}) \, \mathrm{d}s, \tag{A11}$$

which represents the rate at which H is delivered to the RA with the IVC flow. The same methods are applied to calculate the SVC KE flux ($\dot{E}_{SVC}$) and H flux ($\dot{H}_{SVC}$).

To take into account the various waveforms of these haemodynamic quantities over a cardiac cycle, the cyclic averaged (or overall) E_k and E_s contents are calculated as

$$\langle E_k \rangle = \int_{Cyl.} E_k(t) \, \mathrm{d}t \tag{A12}$$
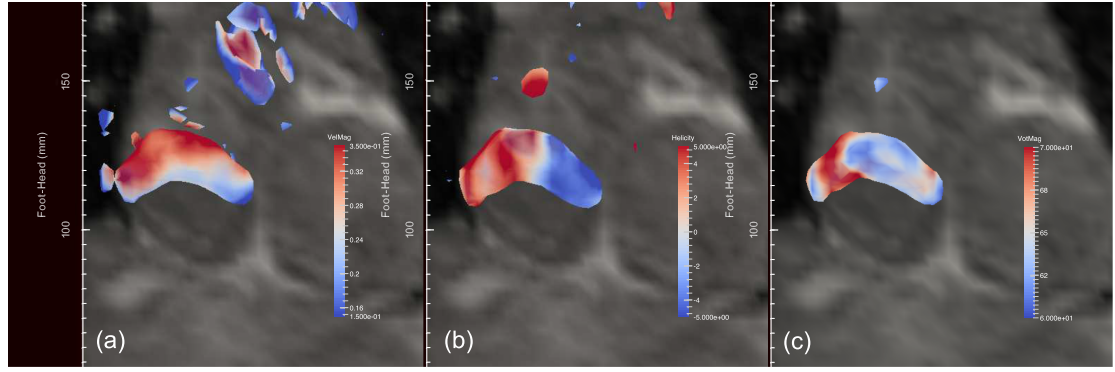
Figure B1. Vortex identification methods. Example shows a single vortex case at peak systole. (a) Flow structure is shown by vorticity magnitude $|\omega|$ criterion. The isosurface is coloured by the local velocity magnitude. The boundary layer built up along the ascending aorta is also seen. (b) Q criterion with isosurface coloured by the local helicity intensity. (c) λ_{ci} criterion, with isosurface coloured by the local $|\omega|$. The isosurface levels chosen in (a)–(c) are arbitrary.

$$\langle E_s \rangle = \int_{\text{Cyl.}} E_s(t)\, \mathrm{d}t, \tag{A13}$$

where E_s and E_k are calculated by equation (A1) and (A3), respectively. Similarly, for dissipation,

$$\langle E_\epsilon \rangle = \int_{\text{Cyl.}} E_\epsilon(t)\, \mathrm{d}t, \tag{A14}$$

with E_ϵ calculated by equation (A6), and for helicity magnitude

$$\langle |H| \rangle = \int_{\text{Cyl.}} |H|(t)\, \mathrm{d}t, \tag{A15}$$

with H calculated by equation (A4).

Appendix B. Vortex identification methods

The RA vortex structure is confirmed by three independent vortex identification method as shown in figure B1. Vorticity $\bar{\omega}$ is the spinning rate of flow particles around itself and is defined by equation (A2). It is a standard way to quantify the rotational strength of a flow. A clear coherent vortex structure can be visualised in the RA as shown in figure B1(a). However, ω does not differentiate a truly rotating flow from a simple parallel flow but with shear (velocity gradient). The latter can typically be seen in a flow inside a pipe close to the inner wall. The shear is cause by the zero flow velocity on the pipe wall and the finite flow velocity in the pipe central region. This shear layer is often called boundary layer and have high vorticity intensity. A boundary layer can clearly be seen to develop along the ascending aorta wall during the peak systole.

Figure B1(b) uses the so-called Q criterion (Kolář V 2007) to visualise vortex structure, defined as

$$Q = \frac{1}{2}\left(\left\| \bar{\Omega}_{ij} \right\|^2 - \left\| \bar{S}_{i,j} \right\|^2 \right), \tag{B16}$$

where $\bar{S}_{ij}$, the strain rate tensor, is defined in equation (A8) and $\|\cdot\|$ denotes tensor magnitude. $\bar{\Omega}_{ij}$ is the rotation rate tensor, defined as

$$\bar{\Omega}_{ij} = \frac{1}{2}\left(\frac{\partial \bar{u}_i}{\partial x_j} - \frac{\partial \bar{u}_j}{\partial x_i} \right). \tag{B17}$$

Q represents the local relative strength of strain and rotation. It defines the vortex as regions where the rotational strength is greater than the strain rate.

Another widely used criterion for vortex identification is λ_{ci} (Zhou *et al* 1999), which quantifies the local swirling strength in a flow. It is based on the decomposition of the velocity gradient tensor ($\nabla \bar{u}$) as

$$\nabla u = \begin{bmatrix} \bar{v}_r & \bar{v}_{cr} & \bar{v}_{ci} \end{bmatrix} \begin{bmatrix} \lambda_r & 0 & 0 \\ 0 & \lambda_{cr} & \lambda_{ci} \\ 0 & -\lambda_{ci} & \lambda_{cr} \end{bmatrix} \begin{bmatrix} \bar{v}_r & \bar{v}_{cr} & \bar{v}_{ci} \end{bmatrix}^T, \tag{B18}$$

where ∇ is the operator $\left(\dfrac{\partial}{\partial x_1}, \dfrac{\partial}{\partial x_2}, \dfrac{\partial}{\partial x_3} \right)$. λ_r is the real eigenvalue with the corresponding eigenvector $\bar{v}_r$ and $\lambda_{cr} \pm \lambda_{ci}$ is the complex conjugate pair of the (complex) eigenvalues with the corresponding eigenvectors $\bar{v}_{cr} \pm \bar{v}_{ci}$. A vortex is present when the eigenvalues $\lambda_{cr} \pm \lambda_{ci}$ exist and the swirling strength of the vortex is reflected by the magnitude of λ_{ci}.

All the three criteria allow objective quantification and visualisation of vortices, if any, although thresholds need to be set in order to remove the background. Using the Q and λ_{ci} methods also discriminate the ascending aorta boundary layer, so are ideal for the current study. It can be shown that the three criteria display a coherent vortex nearly the same shape, suggesting the truly existence of coherent vortex flow pattern in the RA.

ORCID iD

Lian Gan https://orcid.org/0000-0002-4948-4523

References

Arvidsson M, Kovâcs S, Töger J Borgquist R Heiberg E Carlsson M and Arheden H 2016 Vortex ring behaviour provides the epigenetic blueprint for the human heart *Sci. Rep.* **6** 22021

Arvidsson P, Töger J, Heiberg E, Carlsson M and Arheden H 2013 Quantification of left and right atrial kinetic energy using four-dimensional intracardiac magnetic resonance imaging flow measurements *J. Appl. Physiol.* **114** 1472–81

Bloch K, Carlsson M, Arheden H and Stahlberg F 2009 Quantifying coronary sinus flow and global LV perfusion at 3T *BMC Medical Imaging* **9** PMID: 19519892 PMCID: PMC2702273

Carlsson M, Heiberg E, Töger J and Arheden H 2012 Quantification of left and right ventricular kinetic energy using four-dimensional intracardiac magnetic resonance imaging flow measurements *Am. J. Physiol. Heart. Circ. Physiol.* **302** H893–H900

Carlsson M, Töger J, Kanski M, Bloch K, Stahlberg F, Heiberg E and Arheden H 2011 Quantification and visualization of cardiovascular 4D velocity mapping accelerated with parallel imaging or k-t BLAST: head to head comparison and validation at 1.5 T and 3 T *J. Cardiovascular Magn. Reson.* **13** 55

Dabiri J and Gharib M 2005 The role of optimal vortex formation in biological fluid transport *Proc. Royal Society of Biological Sciences* **272** 1557–60

Eriksson J, Dyverfeldt P, Engvall J, Bolger A, Ebbers T and Carlhäll C 2011 Quantification of presystolic blood flow organization and energetics in the human left ventricle *Am. J. Physiol. Heart. Circ. Physiol.* **300** H2135–H2141

Fluckiger J, Goldberger J, Lee D, Ng J, Lee R, Goyal A and Marki M 2013 Atrial flow velocity distribution and flow coherence using four-dimensional flow MRI: a pilot study investigating the impact of age and pre- and postintervention atrial fibrillation on atrial hemodynamics *J. Magn. Reson. Imaging* **38** 580–7

Fyrenius A, Wingström L, Ebbers T, Karisson M, Engvall J and Bolger A 2001 Three dimensional flow in the human left atrium *Heart* **86** 448–55

Gülan U, Saguner A, Akdis D, Gotschy A, Manka R, Brunckhorst C, Holzner M and Duru F 2017 Investigation of atrial vortices using a novel right heart model and possible implications for atrial thrombus formation *Sci. Rep.* **7** 16772

Hong G *et al* 2008 Characterisation and quantification of vortex flow in the human left ventricle by contrast echocardiography using vector particle image velocimetry *JACC Cardiovascular Imaging* **1** 705–17

Kilner P 2010 Letter to the editor: Postulated functional advantages of a looped as opposed to a linearly arranged heart *Am. J. Physiol. Heart. Circ. Physiol.* **298** H726

Kilner P, Henein M and Gibson D 1997 Our tortuous heart in dynamic mode—an echocardiographic study of mitral flow and movement in exercising subjects *Heart Vessels* **12** 103–10

Kilner P, Yang G, Wilkes A, Mohiaddin R, Firmin D and Yacoub M 2000 Asymmetric redirection of flow through the heart *Nature* **404** 759–61

Kolář V 2007 Vortex identification: New requirements and limitations *Int. J. Heat Fluid Flow* **28** 638–52

Maceira A, Cosin-Sales J, Roughton M, SK P and DJ P 2013 Reference right atrial dimensions and volume estimation by steady state free precession cardiovascular magnetic resonance *J. Cardiovascular Magn. Reson.* **15** 15–29

Markl M, Carr M, Ng J, Lee D, Jarvis K, Carr J and Goldberger J 2016 Assessment of left and right atrial 3Dd hemodynamics in patients with atrial fibrillation: a 4D flow MRI study *Int. J. Cardiovascular Imaging* **32** 807–15

Markl M, Frydrychowicz A, Kozerke S, Hope M and Wieben O 2012 4D flow MRI *J. Cardiovascular Magn. Reson.* **36** 1015–36

Markl M, Kilner P and Ebbers T 2011 Comprehensive 4D velocity mapping of the heart and great vessels by cardiovascular magnetic resonance *J. Cardiovascular Magn. Reson.* **13**

Martínez-Legazpi P *et al* 2014 Contribution of the diastolic vortex ring to left ventricular filling *J. Am. College Cardiol.* **64** 1711–21

Meng X, Li Y, Li H, Wang Y, Zhu W and Lu X 2017 Right atrial function in patients with pulmonary hypertension: A study with two-dimensional speckle-tracking echocardiography *Int. J. Cardiol.* **255** 200–5

Parikh J, Kakarla J, Keavney B, O'Sullivan J, Ford G, Blamire A, Hollingsworth K and Coats L 2017 4D flow MRI assessment of right atrial flow patterns in the normal heart—influence of caval vein arrangement and implications for the patent foramen ovale *PLoS ONE* **12** e0173046

Pedrizzetti G and Domenichini F 2005 Nature optimises the swirling flow in the human left ventricle *Phys. Rev. Lett.* **95** 108101

Prec O, Katz L, Sennett L, Rosenman R, Fishman A and Hwang W 1949 Determination of the kinetic energy of the heart in man *Am. J. Physiol. – Legacy Content* **159** 483–91

Ruski L, Lai W, Afilado J, Hua L, Handschumacher M, Chandrasekaran K, Solomon S, Louie E and Schiller N 2010 Guidelines for the echocardiographic assessment of the right heart in adults: a report from the american society of echocardiography *J. Am. Soc. Echocardiography* **23** 685–713

Sallach J *et al* 2009 Right atrial volume index in chronic systolic heart failure and prognosis *JACC Cardiovascular Imaging* **2** 527–34

Selton-Suty C and Juilliére Y 2009 Non-invasive investigations of the right heart: how and why? *Archives of Cardiovascular Disease* **102** 219–32

Sheng J, Meng H and Fox R 2000 A large eddy PIV method for turbulence dissipation rate estimation *Chem. Eng. Sci.* **55** 4423–34

Smagorinsky J 1963 General circulation experiments with the primitive equation I the basic experiment *Mon. Weather Rev.* **164** 91–9

Suwa K *et al* 2014 Characteristics of intra-left atrial flow dynamics and factors affecting formation of the vortex flow *Circ. J.* **79** 144–52

Töger J Kanski M Carlsson M Kovacs S Soderlind G Arheden H and Heiberg E 2012 Vortex ring formation in the left ventricle of the heart: analysis by 4D flow MRI and lagrangian coherent structures *Ann. Biomed. Eng.* **40** 2652–2662

Watanabe H, Sugiura S and Hisada T 2008 The looped heart does not save energy by maintaining the momentum of blood flowing in the ventricle *Am. J. Physiol. Heart. Circ. Physiol.* **294** H2191–H2196

Watanabe H, Sugiura S and Hisada T 2010 Reply to Letter to the editor: 'Postulated functional advantages of a looped as opposed to a linearly arranged heart. *Am. J. Physiol. Heart. Circ. Physiol.* **298** H2727

Wehrum T, Lodemann T, Hagenlocher P, Stuplich J, Ngo B, Grundmann S, Hennemuth A, Hennig J and Harloff A 2018 Age-related changes of right atrial morphology and inflow pattern assessed using 4D flow cardiovascular magnetic resonance: results of a population-based study *J. Cardiovascular Magn. Reson.* **20** 38

Zhou J, Adrian R, Balachandar S and Kendall T 1999 Mechanisms for generation coherent packets of hairpin vortices in channel flow *J. Fluid Mech.* **387** 353–96